Tissue self-organization based on collective cell migration by contact activation of locomotion and chemotaxis

Taihei Fujimori[a], Akihiko Nakajima[a,b], Nao Shimada[a], and Satoshi Sawai[a,b,1]

[a]Graduate School of Arts and Sciences, University of Tokyo, Komaba, 153-8902 Tokyo, Japan; and [b]Research Center for Complex Systems Biology, Universal Biology Institute, University of Tokyo, Komaba, 153-8902 Tokyo, Japan

Edited by Herbert Levine, Rice University, Houston, TX, and approved January 22, 2019 (received for review September 14, 2018)

Despite their central role in multicellular organization, navigation rules that dictate cell rearrangement remain largely undefined. Contact between neighboring cells and diffusive attractant molecules are two of the major determinants of tissue-level patterning; however, in most cases, molecular and developmental complexity hinders one from decoding the exact governing rules of individual cell movement. A primordial example of tissue patterning by cell rearrangement is found in the social amoeba *Dictyostelium discoideum* where the organizing center or the "tip" self-organizes as a result of sorting of differentiating prestalk and prespore cells. By employing microfluidics and microsphere-based manipulation of navigational cues at the single-cell level, here we uncovered a previously overlooked mode of *Dictyostelium* cell migration that is strictly directed by cell–cell contact. The cell–cell contact signal is mediated by E-set Ig-like domain-containing heterophilic adhesion molecules TgrB1/TgrC1 that act in trans to induce plasma membrane recruitment of the SCAR complex and formation of dendritic actin networks, and the resulting cell protrusion competes with those induced by chemoattractant cAMP. Furthermore, we demonstrate that both prestalk and prespore cells can protrude toward the contact signal as well as to chemotax toward cAMP; however, when given both signals, prestalk cells orient toward the chemoattractant, whereas prespore cells choose the contact signal. These data suggest a model of cell sorting by competing juxtacrine and diffusive cues, each with potential to drive its own mode of collective cell migration.

cell migration | cell sorting | chemotaxis | cell–cell contact | *Dictyostelium*

One of the fundamental processes that underlie tissue patterning is spatial rearrangement and repositioning of cells according to their cell types (1–3). In vitro studies have demonstrated wide occurrence of cell-type dependent segregation in the mixture of cells dissociated from different tissues (4–6). Such cell segregation has traditionally been explained based on differences in cell–cell adhesion force and surface tension in analogy to phase separation, e.g., of oil and water where membrane fluctuations would drive rearrangement of relative positions of cells so as to minimize total free energy. Quantitative measurements in conjunction with mathematical modeling have successfully provided qualitatively accurate predictions of in vitro sorting patterns (7, 8). While such view of cell segregation does seem to hold for in vitro systems, the extent of their contribution in vivo remains to be questioned. In many cases, such a stochastically driven process appears not to hold, as cells are migratory (9, 10), and segregation occurs rapidly without being trapped in metastable states. In the primitive streak of chicken embryo and limb bud, directed migration is the primary driving force of morphogenesis (11, 12). In zebrafish gastrulation, internalization of mesendoderm cells requires Rac-dependent directed cell migration (9). These examples point to the importance of specific directional cues and migration in cell segregation; however, the exact navigational rules at the single-cell level and their linkage to the resulting tissue patterns are still largely undeciphered.

In the social amoeba *Dictyostelium discoideum*, upwards of 100,000 cells aggregate by chemotaxis to self-generated waves of extracellular cAMP (13–17) to form a multicellular mound. In the mound, cells differentiate into either prespore or prestalk cells that initially appear at random positions before being segregated to form a distinct prestalk tip region (3, 18, 19)—an organizing center that sits on top of a prespore cell mass (Fig. 1*A*). During this process, cAMP waves cease (*SI Appendix*, Fig. S1 *A* and *B*) (20), prespore cells migrate radially while prestalk cells exhibit a combination of radial and centripetal movement toward the apical region (Fig. 1*B*). Several lines of evidence suggest the importance of chemotaxis to extracellular cAMP in cell segregation (21–23). A gradient of extracellular cAMP formed by a glass needle in a mound can direct prestalk cell migration (23), and overexpression of cAMP-specific phosphodiesterase (PDE) suppresses tip formation (21). On the other hand, heterophilic adhesion molecules TgrB1 and TgrC1 (24, 25) are also essential for tip formation (26). Knockout mutant of TgrC1 exhibits motility defects (27) as well as loss of developmental gene expression (26, 28). Moreover, application of antibody against TgrC1 to regenerating mounds suppresses prestalk/prespore segregation (29). TgrB1 and TgrC1 are also known for their polymorphism, which results in kin discriminatory segregation during aggregation (25, 30, 31). These lines of evidence suggest requirement for extracellular cAMP and

Significance

Migration of cells as a group is pivotal to the making of various tissues in developing embryos; however, their complexity hinders one from identifying the exact rules. We exploited relatively simple and conditional multicellularity of the social amoeba *Dictyostelium* to analyze tissue patterning from bottom up by identifying the navigation rules at the individual cell level. We uncovered a guidance mechanism directed by cell–cell contact which gives rise to collective migration and competes with diffusive attractant molecules. Competition of the two directional cues forms the basis of how cells position themselves in the multicellular aggregate according to cell type. A similar scheme of collective migration and sorting may underlie patterning of other developing tissues as well as cancer invasion.

Author contributions: T.F., A.N., and S.S. designed research; T.F. performed research; A.N. and N.S. contributed new reagents/analytic tools; T.F. analyzed data; and T.F. and S.S. wrote the paper.

The authors declare no conflict of interest.

This article is a PNAS Direct Submission.

This open access article is distributed under Creative Commons Attribution-NonCommercial-NoDerivatives License 4.0 (CC BY-NC-ND).

[1]To whom correspondence should be addressed. Email: cssawai@mail.ecc.u-tokyo.ac.jp.

This article contains supporting information online at www.pnas.org/lookup/suppl/doi:10.1073/pnas.1815063116/-/DCSupplemental.

Published online February 19, 2019.

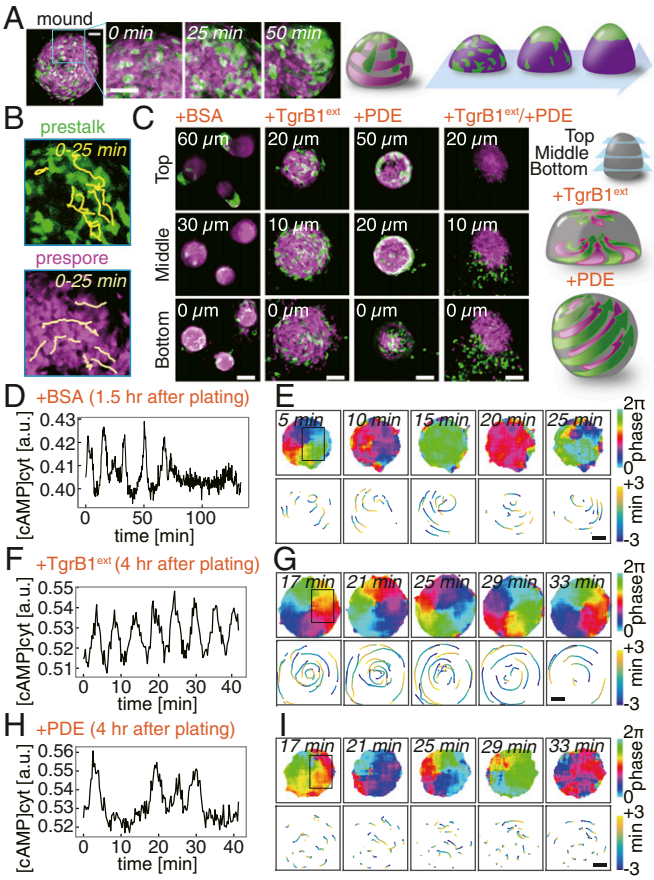

Fig. 1. Two navigational cues and the modes of collective movement underlie segregation of prestalk and prespore cells in a *Dictyostelium* mound. (*A*) Tip formation (green, prestalk marker ecmAOp:GFP; magenta, prespore marker D19p:RFP). (Scale bars, 50 μm.) (*B*) Cell trajectories (*Upper*, prestalk cells; *Lower*, prespore). (*C–I*) Interference of tip regenerating cues (*SI Appendix*, Fig. S1*E* and Movie S1). Z sections taken at 3 h 40 min after plating (+BSA mock control, +TgrB1^{ext}, +PDE, +TgrB1^{ext}/+PDE) (*C*). (Scale bars, 50 μm.) Schematic illustrations of cell motion (*Right*). (*D–I*) Time series of the mean cytosolic cAMP levels (*D*, *F*, and *H*) in boxed regions (*E*, *G*, and *I*, *Upper Left*). Cell trajectories [98% Epac1-camps/AX4 (16): 2% Lifeact-RFP/AX4 cells; +BSA (*D* and *E*), +TgrB1^{ext} (*F* and *G*), +PDE (*H* and *I*)]. Phase of the cAMP oscillations (*E*, *G*, and *I*, *Upper*) (15). Trajectories of RFP-labeled cells during one cycle of the oscillation (*E*, *G*, and *I*, *Lower*). (Scale bars, 20 μm.)

TgrB1/C1 for tip formation; however how they dictate the cell segregation process remains to be resolved (3, 32).

Results

Navigational Cues for *Dictyostelium* Cell Migration. To study how cell migration is being directed in the mound, we analyzed the effect of interfering with extracellular cAMP and TgrB1/C1. To circumvent developmental effects due to the requirement of TgrB1/C1 on cell differentiation (26), we took advantage of the fact that the process is entirely self-organizing, i.e., it can be recapitulated by fully differentiated prestalk and prespore cells after dissociation (33). Dissociated cells plated on an agar plate, immediately began emitting cAMP waves, reaggregated, and then formed tips as cAMP waves ceased (Fig. 1 *C–E*, *SI Appendix*, Fig. S1*A*, and Movie S1). When regenerating mounds were immersed in purified TgrB1^{ext} (*SI Appendix*, Fig. S1 *C–F*), cAMP wave propagation did not stop, and cells moved in a highly coordinated scrolling motion at least for the duration of our observation (Fig. 1 *F* and *G*). Prestalk and prespore cells moved similarly and did not segregate (Fig. 1*C*, +TgrB1^{ext}; Movies S1 and S2). Addition of purified TgrC1^{ext} resulted in a loose mound that cycles between cell aggregation and dispersal, but tips eventually formed after a 2-h delay (*SI Appendix*, Fig. S1 *F–H* and Movies S1 and S2). When exposed to cAMP-specific PDE to attenuate extracellular cAMP, mounds became spherical, and the cells continued to migrate radially as the entire cell mass moved like a rolling ball (Fig. 1*C*, +PDE; Movies S1 and S2). Prestalk cells sorted out to the periphery but never collected to form the apical tip (Fig. 1*C*, +PDE; *SI Appendix*, Fig. S1*G*). The rotational movement was not correlated with a few passages of residual waves (Fig. 1 *H* and *I*), suggesting that cell migration, despite being highly coordinated, was not chemotactically oriented. When both purified TgrB1^{ext} and PDE were applied, prestalk cells were completely stalled, while prespore cells retained some movement but were less coordinated (Fig. 1*C*, +TgrB1^{ext}/+PDE; Movie S1). These observations indicate that, in addition to chemotaxis toward cAMP, there is an additional guidance cue mediated by cell–cell contact that directs collective cell movement.

TgrB1/C1 are essential for postaggregative gene regulation and are differentially expressed in pretalk and prespore cells (*SI Appendix*, Fig. S2) (26, 28). To avoid developmental effects and clarify the basic rule of cell movement, we first analyzed migration of cells immediately before prestalk/prespore diversification ("streaming-stage" cells; see *Materials and Methods*) using a microfluidic gradient chamber (*SI Appendix*, Fig. S3 *A* and *B*). While moving toward the cAMP source, cells made head-to-tail contacts and formed trains (Fig. 2*A* and Movie S3). At low loading densities, most cell trains were short; many consisted of two cells (Fig. 2*B*). In both two-cell and longer cell trains, leader cells formed lateral pseudopods and exerted exploratory trajectories similar to solitary migration, whereas those that followed were elongated, monopodal, and moved ballistically (Fig. 2*C* and *SI Appendix*, Figs. S3 *C–F* and S4). To delineate the role of chemotaxis and cell–cell contact, response to a reorienting cAMP gradient was analyzed (*SI Appendix*, Fig. S5). Within minutes after gradient reversal, solitary cells and leader cells changed their direction by extending de novo pseudopods (Fig. 2*D*, *Upper*). While some follower cells also responded similarly, many exhibited no immediate response and continued to follow the cell in contact (Fig. 2*D*, *Lower*, Fig. 2*E*, and Movie S4). Given that the cells were treated here with adenylyl cyclase inhibitor SQ22536 (16, 34) to suppress cAMP synthesis, these observations suggest that in addition to chemotaxis to cAMP required for the formation of cell streams (35), there may be an alternative mode of navigation that depends on cell–cell contact.

F-Actin Dynamics at Cell–Cell Contact Sites. Compared with transient formation of F-actin at the leading edge without cell contact (Fig. 2*F*, *Left*, magenta) (36), F-actin at the cell–cell contact was persistent, long (~5 μm), and appeared most strongly at the outer edge (Fig. 2*F*, *Right*, magenta, *SI Appendix*, Fig. S6*A*, and Movie S5). The F-actin pattern was also observed in naturally streaming cells (*SI Appendix*, Fig. S6*B*). The contact region was highly enriched in Arp2/3 (Fig. 2*G*), indicating that actin filaments form dendritic networks (37). These observations are compatible with the general feature of a leading edge of migrating cells where dendritic F-actin networks grow mainly by side-branching nucleation mediated by the Arp2/3 complex, while further away toward the cytosolic region, filaments are severed and depolymerized. The other widespread feature of the leading edge in various cells is the so-called "retrograde" flow of F-actin due to excess filament growth relative to the speed of membrane expansion. Although solitary migrating *Dictyostelium* cells are known to lack obvious retrograde flow at the leading edge (38), time-lapse images of F-actin at the cell–cell contact region were indicative of such flow (Movie S5). To quantitate the speed of retrograde flow of the F-actin network, GFP-Arp2 incorporated in dendritic filaments was photobleached partially, and dislocation of the bleached region was followed over time. After photobleaching of GFP-Arp2, the nonfluorescent region moved backward (Fig. 2 *G* and *H*) at about 14 μm/min in cell-contacted leading edge compared with 1 μm/min (Fig. 2*I*) in cell

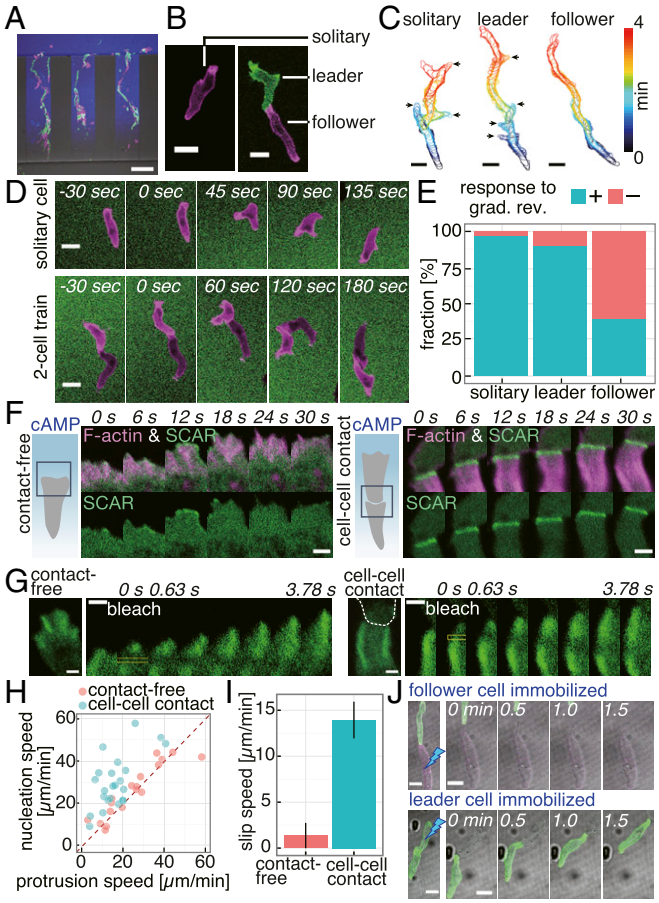

Fig. 2. Microfluidics single-cell level analysis of train migration and contact-induced leading edge dynamics. (*A*) Train migration. GFP-Lifeact/AX4 (green), Lifeact-RFP/AX4 (magenta), 0- to 10-nM cAMP gradient (blue, ATTO425). (Scale bar, 100 μm.) (*B*) Snapshots of solitary (*Left*) and two-cell train (*Right*). (Scale bar, 10 μm.) (*C*) Cell contours (arrows, lateral pseudopods). (Scale bars, 10 μm.) (*D*) Response to reversal of cAMP gradient (0–1 μM; magenta, Lifeact-RFP; green, fluorescein). (Scale bars, 10 μm.) (*E*) Fraction of cells with (+) or without (−) an immediate response (solitary: n = 73 cells, leader: n = 28 cells, follower: n = 97 cells). (*F*) A contact-free (*Left*) and a cell–cell contact (*Right*) leading edge (green, HSPC300-GFP and magenta, Lifeact-RFP) in a 0- to 1-μM cAMP gradient. (Scale bars, 2 μm.) (*G*) Fluorescence recovery after photobleaching in GFP-Arp2/AX4 cells (yellow boxed region) in a contact-free (*Left*) and contacted (*Right*) leading edge. White dashed line, a leading cell contour; 0- to 10-nM cAMP gradient. (Scale bars, 1 μm.) (*H*) Scatterplot of nucleation and protrusion speed. (*I*) Slip speed of actin filaments. Mean ± SEM, contact-free: n = 18 cells, cell–cell contact: n = 23 cells. (*J*) Immobilization of a follower (*Upper*) or a leader (*Lower*) by UV irradiation; 0- to 10-nM cAMP gradient. (Scale bars, 10 μm.)

contact-free leading edge, suggesting an enhanced nucleation at the contact site.

The enhanced F-actin formation at the cell-contacted leading edge suggests that there is up-regulation of Arp2/3 activity. In solitary migrating *Dictyostelium* cells, the SCAR complex, which is required for full activation of the Arp2/3 complex, translocated to the membrane in small patches that lasted no longer than ∼10 s (36) (Fig. 2*F*, *Left*, magenta). In contrast, at the cell-contacted leading edge, there was markedly enhanced localization of the SCAR complex (Fig. 2*F*, *SI Appendix*, Fig. S6 *C* and *D*, and Movie S5). Transient localization of myosin II during the short-term retraction of the leading edge in solitary cells (*SI Appendix*, Fig. S7*A*) was completely absent from the leading edge of follower cells (*SI Appendix*, Fig. S7 *B–E*). Major leading-edge signals such as Ras-GTP, PI(3,4,5)P3, and Rac-GTP were also present at the contacted front and appeared similar to contact-free leading edge (*SI Appendix*, Fig. S6 *E–J*). These observations suggest that the follower cells have a leading edge with a persistent dendritic F-actin network that generates unidirectional propulsive force that pushes the plasma membrane forward. Accordingly, when leader cells were immobilized by UV irradiation, the follower cells continued to move and push the leader cells (Fig. 2*J* and Movie S6). The observation indicates contact-dependent protrusive activity that is independent of pulling by the front cell in contact. The cell–cell contact mode of migration was also evident in the slug-stage cells, as they exhibited train migration in a microchamber with the characteristic SCAR complex localization at the contact site and the ballistic motion of follower cells (*SI Appendix*, Fig. S8*A*). In addition to head-to-tail contact as observed in streaming-stage cells, head-to-head was frequently observed in slug-stage cells (*SI Appendix*, Fig. S8*B*). As in streaming-stage cells, transient localization of myosin II at the contact-free front was absent from the cell-contacted front in slug-stage cells (*SI Appendix*, Fig. S8*C*).

TgrB1/C1 and Contact-Induced Front Protrusion. The molecular basis of cell-train formation was further analyzed by studying binary mixtures of WT, *tgrB1*⁻, and *tgrC1*⁻. First, streaming-stage cells were employed to circumvent the inability of the Tgr-null cells to differentiate after aggregation (28). We found that in cells that follow *tgrC1*⁻, F-actin formation failed to become persistent (Fig. 3 *A* and *B* and *SI Appendix*, Fig. S9 *A* and *B*). The pairwise frequency of the contact itself was also low when cells being followed were *tgrC1*⁻ or when the following cells were *tgrB1*⁻ (Fig. 3*C*), which is consistent with a recent study suggesting that TgrB1 and TgrC1 act as a receptor and a ligand, respectively, for allorecognition (31). TgrB1/C1 are developmental stage-specific genes, hence the protrusions and the elongated shape in developing cells were never induced by contact with vegetative cells unless TgrC1 was overexpressed (Fig. 3*D* and *SI Appendix*, Fig. S9 *C* and *D*). Moreover, streaming-stage cells were able to follow TgrC1 overexpressing vegetative cells that migrated toward their chemoattractant folate (Fig. 3*E* and Movie S7). Since vegetative cells do not secrete cAMP nor do the streaming-stage cells chemotax to folate, contact-dependent front protrusion and guidance are mediated primarily by TgrB1/C1 and do not require chemoattraction.

In the case of slug-stage cells, cells formed small clusters without a stable contact-free front and rotated in random directions (*SI Appendix*, Fig. S10). Application of purified TgrB1^{ext} in a cAMP gradient extinguished the cell clusters and cells migrated directionally along the cAMP gradient (*SI Appendix*, Fig. S10*A* and Movie S8). Furthermore, silica beads coated with purified TgrC1^{ext} and lectin wheat germ agglutinin (WGA) which binds to cell surface glycoproteins such as the homophilic adhesion protein CsA (39) were able to induce an extensive protrusion at the site of cell–microsphere contact (Fig. 3*F*). Much like in cell trains, the cell–microsphere contact site was intensely decorated with the SCAR complex and F-actin (Fig. 3*F* and Movie S9). Microsphere coated with WGA alone or TgrC1^{ext} alone or TgrB1^{ext}/WGA was unable to induce the characteristic protrusion (*SI Appendix*, Fig. S11*A*). The results indicate that juxtacrine signaling between TgrC1 at the tail of a cell and TgrB1 at the front of a cell activates the SCAR complex and induces a highly enhanced formation of F-actin at the cell–cell contact site. The induction by the TgrC1^{ext}/WGA-coated beads was also observed in streaming-stage cells (*SI Appendix*, Fig. S11 *B* and *C*) but was less frequent.

Despite their spatially restricted mechanism of action, TgrB1 was localized to the front and the back of collectively moving cells in a mound, whereas TgrC1 was observed uniformly at the plasma membrane (Fig. 3*G* and *SI Appendix*, Fig. S12 *A–C*). Lack of front/back symmetry breaking was puzzling, considering that, in cell trains and mounds, cells did not form two fronts in the opposing directions. In cells attached to two beads, cells indeed formed a front protrusion on one bead, and the other bead was attached to their tail except in cases where protrusions faced the same directions and hence cells were double headed

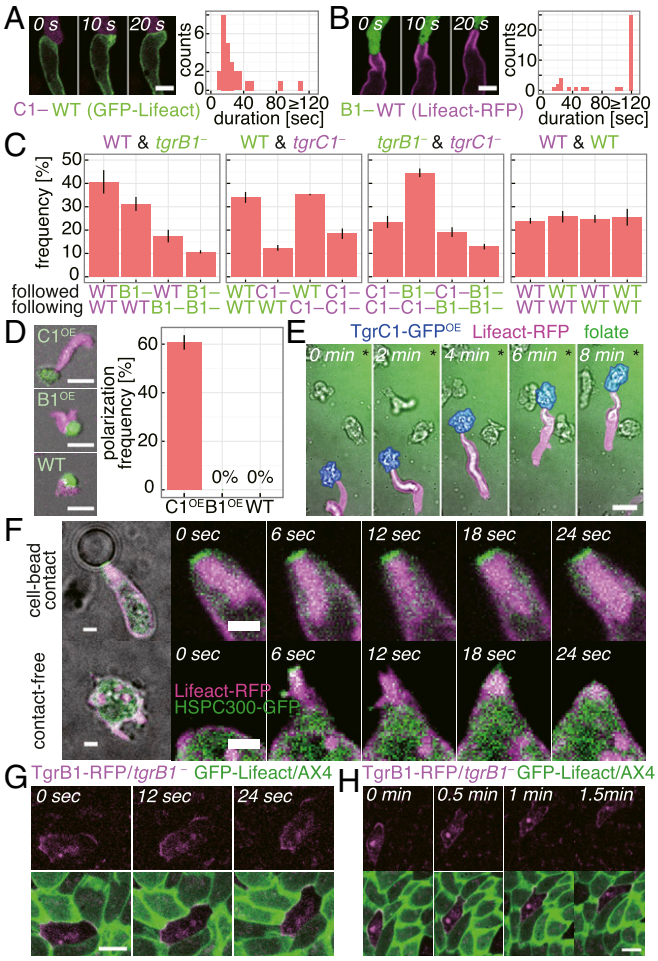

Fig. 3. Contact-based front protrusion and train migration is mediated by TgrB1/TgrC1 interaction. (*A* and *B*) Contact-induced F-actin formation [*Left*; C1–: tdTomato/*tgrC1*$^{-}$ (*A*), B1–: GFP/*tgrB1*$^{-}$ (*B*), WT: AX4] and their duration [*Right*; $n = 26$ events (*A*), $n = 38$ events (*B*)]. (Scale bar, 5 μm.) (*C*) Occurrence of head-to-tail contacts in 1:1 mixtures of GFP/*tgrB1*$^{-}$ (B1–, green), tdTomato/*tgrC1*$^{-}$ (C1–, magenta), Lifeact-RFP/AX4 (WT, magenta) and GFP-Lifeact/AX4 (green) (mean ± SEM; $n = 3$ trials each; 120 ~ 405 pairs total). (*D*) Streaming-stage Lifeact-RFP/AX4 cells (magenta) attached to vegetative cells overexpressing TgrC1-GFP (*Upper Left*), TgrB1-RFP (*Middle Left*; CellTrackerGreen), or GFP-Lifeact (*Lower Left*). Occurrence of protrusions at the contact site [*Right*; mean ± SEM; $n = 3$ trials; total 49(C1^{OE}), 46(B1^{OE}), 16(WT) pairs]. (Scale bars, 20 μm.) (*E*) A streaming-stage Lifeact-RFP/AX4 cell (magenta) in contact with a vegetative-stage TgrC1-GFP overexpressing cell (blue) in a folate gradient (green, fluorescein; * source direction). (Scale bar, 10 μm.) (*F*) Slug-stage HSPC300-GFP/Lifeact-RFP/AX4 cells attached to a TgrC1^{ext}/WGA-coated microsphere (*Upper*) or in isolation (*Lower*) in a microchamber. (Scale bars, 2 μm.) (*G* and *H*) A chimeric monolayer of TgrB1-RFP/*tgrB1*$^{-}$ (magenta) and GFP-Lifeact/AX4 (green) in a microchamber. (Scale bar, 10 μm.) Splitting of a TgrB1-RFP enriched leading edge (*H*, 0.5 min) and selection of a single contact site (*H*, 1.5 min).

(*SI Appendix*, Fig. S12*D*). These results suggest that a protrusion is inhibited from forming at the tail once cells polarize. Interestingly, the choice of a bead to which protrusion formed sometimes swapped between the two (*SI Appendix*, Fig. S12*E*), suggesting that contact-mediated polarity is dynamically maintained and possibly mechanosensitive. Similar front competitions were often observed in a monolayer aggregate where TgrB1 first accumulated toward two cells which then split as the cells deviated, and a contact with one cell was selected (Fig. 3*H* and Movie S10).

Single-Cell-Level Response to Navigational Cues. Lastly, slug-stage cells were analyzed in details according to the cell types to delineate the roles of chemotaxis and contact-dependent protrusion in tip formation. It has been hypothesized that prestalk cells sort to the tip by migrating fast and winning the chemotaxis race against prespore cells (22, 32). When assayed at the single-cell level, however, prespore cells migrated faster than prestalk cells in a 0- to 1-μM cAMP linear gradient (Fig. 4*A*). Similar results were obtained from tracking well-isolated dissociated cells in the initial phase of reaggregation mitigated of contact signal by TgrB1^{ext} (Fig. 4*B*). In a 0- to 10- or 0- to 50-μM linear gradient, both cell types halted at the same location in the channel, indicating a similar response range (*SI Appendix*, Fig. S13). How then can cell–cell contacts facilitate cell segregation? When attached to TgrC1^{ext}/WGA-coated microsphere (Fig. 4*C*), a marked protrusion was observed in about one-third of the cell–bead interface regardless of the cell type (Fig. 4*D*). While the prespore cells exhibited a single protrusion at the contact site, many of the prestalk cells had auxiliary protrusions (Fig. 4*C*, arrows, Fig. 4*E*, and Movie S11). Accordingly, in two-cell clusters, Arp2 accumulated at multiple contact sites in prestalk cells, whereas in prespore cells it was confined to a single contact site (*SI Appendix*, Fig. S8*D*). The difference in the number of protrusions between prespore and prestalk cells was also evident in vivo and in isolation without cell–cell contact (*SI Appendix*, Fig. S14). When exposed to a cAMP gradient, the protrusion of prestalk cells at the bead–cell interface often disappeared and new pseudopods formed toward the cAMP source, whereas prespore cells remained attached to the beads and retained the polarity (Fig. 4 *F* and *G* and Movie S12). The results indicate that prestalk and prespore can be oriented by cAMP and TgrB1/C1; however, when both signals are presented, there is a dominance as to which directs their leading edge. Prestalk cells are

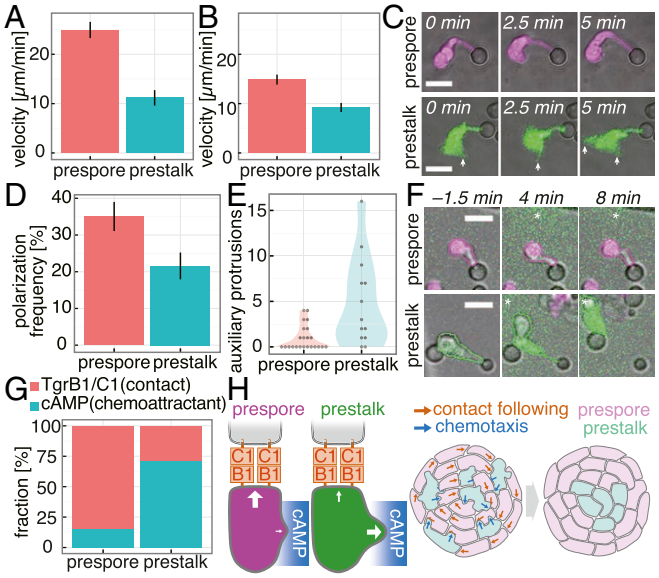

Fig. 4. Single-cell level analysis of migratory response to navigational cues. (*A*) Speed of isolated single cells in 0- to 1-μM cAMP gradient (mean ± SEM, prespore: $n = 33$ cells, prestalk: $n = 10$ cells). (*B*) Speed of single cells during reaggregation in the presence of purified TgrB1^{ext} (mean ± SEM, prespore: $n = 28$ cells, prestalk: $n = 19$ cells). (*C*) A prestalk (green, GFP) and a prespore (magenta, RFP) cell attached to a TgrC1^{ext}/WGA-coated microsphere. Prestalk cells form lateral protrusions (arrows). (Scale bars, 10 μm.) (*D*) Frequency of cell–bead contact-dependent polarization (mean ± SEM; $n = 3$ trials). (*E*) Number of lateral protrusions formed in cells attached to beads and elongated within 5 min (prespore: $n = 23$ cells, prestalk: $n = 13$ cells). (*F*) Polarized cells attached to beads stimulated with a cAMP gradient (green, fluorescein; * source direction). (Scale bars, 10 μm.) (*G*) Percentage of cells that maintain Tgr-mediated polarity (TgrB1/C1) or abort the contact by protruding toward a cAMP gradient (cAMP). Prespore: $n = 19$ cells, prestalk: $n = 7$ cells. (*H*) A schematic illustration of the cell navigation rule.

less polarized, continue to form random pseudopods even in the presence of a Tgr-induced protrusion, and thus can be navigated chemotactically, whereas prespore cells are highly polarized and locked in toward the cell–cell contact. Taken together with the results demonstrating requirements for two cues TgrC1 and cAMP for tip formation (Fig. 1 *C–H*), the radial trajectories and the head-to-tail alignment of prespore cells is best explained by the Tgr-mediated navigation, whereas prestalk cells deviate from the contact-mediated collective migration and chemotax to extracellular cAMP (Fig. 4*H*).

Discussion

A propensity of *Dictyostelium* cells to follow cells in contact was suggested by a classic work by Shaffer who coined the term "contact following" (40); however, it has remained heretofore unclear (41, 42). In the present work, we conclude that the following behavior is driven by "contact activation of locomotion"—an induction of leading edge by cell–cell contact and the accompanying forward propulsion. The cell-contacted leading edge was highly enriched in a SCAR complex subunit HSPC300 and dendritic F-actin. Since the same response was observed in cells attached to TgrC1^{ext}/WGA-coated microspheres, there appears to be a mechanism whereby TgrB1/C1 interaction induces accumulation of the SCAR complex at the cell–cell contact site. Lack of apparent features in the cytosolic residues in TgrB1 and requirement for lectin WGA for the response points to a possibility that the interaction between TgrB1 and the SCAR complex is indirect and that there is clustering of adhesion and signaling complex at the contact site. The contact site appears distinct from that forming a phagocytic cup, since the contact area appears to extend narrowly instead of expanding and engulfing. A PI(3,4,5)P3 marker, PHcrac-RFP, known to be enriched in phagocytic cups (43) was not localized at the cell–bead interface (*SI Appendix*, Fig. S15 *A* and *B*). Addition of latrunculin A shortened the protrusion; however, it did not promote bead engulfment (*SI Appendix*, Fig. S15*C*). Retrograde flow of F-actin has been suggested to play a major role in determining front–back polarity and its persistence during cell migration (44). In addition, it has been shown that F-actin flow induced by confinement and decrease in cell–substrate adhesiveness helps to establish persistent cell polarity by rearward transfer of inhibitors for protrusion such as myosin II (45). The observations of the retrograde flow, absence of myosin II at cell-contacted front, monopodal morphology, and loss of cell–substrate adhesion in the cell anterior are in line with the current understanding of strong cell polarity in migrating cells.

Expression of TgrB1/C1 begins in the aggregation stage, and the observed contact activation of locomotion and the resulting directionality in streaming-stage cells is consistent with an earlier observation that TgrC1-null cells segregate from the wild type during aggregation in the chimeric mixtures (46). In the post-aggregation stage, our results indicate that the contact signal has cell type-specific effect on the directionality of cell migration. It is essential for prestalk/prespore segregation as evidenced by well-mixed distribution of cells in a mound when contact signal was interfered with purified TgrB1^{ext} (Fig. 1*C*). A protrusion at the contact site appears Tgr dependently in both prestalk and prespore cells; however, this appears to occur on top of a base difference in the degree of cell polarity that exists in the absence of cell–cell contact (*SI Appendix*, Fig. S14 *D* and *E*). In mammalian cells, dominance of a single-cell protrusion requires abundance of myosin II-enriched actin cortex (47). Indeed, in cells that had Arp2 pharmacologically removed, thus free of potential bias by F-actin flow and motility, the level of cortical myosin II was higher in prespore cells than prestalk cells (*SI Appendix*, Fig. S8*E*). In line with earlier genetics studies that showed that a null mutant of myosin II (48) or myosin regulatory chain fails to form the mound tip (19), the present results highlight the importance of polarity difference for cell segregation. While sorting of prestalk cells to the mound periphery in the presence of PDE can be due to prestalk cells being weakly cohesive (49), our data suggest that it accompanies their lesser ability to become monopodal and thus migrate directionally by contact.

Given the fact that prestalk cells showed higher level of TgrB1/C1 (*SI Appendix*, Fig. S2*G*), and clones with overly high levels of TgrC1 were unable to join the aggregates (*SI Appendix*, Fig. S2*H*), a limited supply of TgrB1/C1 and their subcellular clustering may be of importance for a cell to selectively follow a single cell and hence to correctly reposition itself within a multicellular mass. Lack of chemotactic response by the polarized prespore cells can be understood from its inability to engage in the pseudopod-driven chemotaxis (50) whereby randomly generated pseudopods are selected for dominance based on the local chemoattractant concentrations. On the other hand, the present study does not rule out complex in vivo mechanisms based on the occupancies of cAMP receptors and TgrB1. cAMP receptor *carB* and *carD* are expressed specifically in prestalk cells while *carA* and *carC* are more highly expressed in prespore cells (*SI Appendix*, Fig. S2 *A–F*) (51). Knockout of the *carB* gene has been known to exhibit aberrant tips and severely delayed slug formation (52); however, a recent study suggested that the aberrant phenotype may be strain dependent (53). Further studies are needed to clarify the molecular basis of cell polarity and chemotaxis difference in prespore and prestalk cells.

The mechanism of collective migration in *Dictyostelium* uncovered in this study is in striking contrast to that of the neural crest cells. There, cell–cell contact signal mediated by cadherin activates RhoA, inhibits protrusion, and facilitate cell repulsion (54). On the other hand, migration toward self-secreted chemoattractant C3a keeps neural crest cells together (55, 56). In *Dictyostelium*, cell–cell contact mediated by TgrB1/C1 promotes protrusion, and chemotaxis rather is disruptive to otherwise more tightly packed cell mass as evidenced by mounds becoming spherical in the absence of the chemotactic cue. The present findings raise many open questions for future work. Besides prestalk segregation, the migratory mechanism may be relevant to *Dictyostelium* slug migration, culmination as well as kin-discriminatory segregation (25, 30). Also of note is a striking evolutionary convergence of collective cell migration, despite no homologs of TgrB1/C1 existing in metazoans. Are there parallelisms to protocadherin-dependent SCAR complex recruitment and enhancement of migration in cultured cells (57) or similar enhancement of F-actin by atypical cadherin in rotating the *Drosophila* egg chamber (58)? Are other cell-streaming behaviors such as those observed in human breast cancer cells (59) driven by a related mechanism? Drawing from a recent demonstration of contact following in tissue culture cells (60), it is tempting to speculate that contact activation of locomotion is at work in systems outside of *Dictyostelium*. Further investigations in these phenomena should clarify common rules and logical necessities for cellular collectivity.

Materials and Methods

Cell Preparation, Microfluidics, and Live Cell Imaging. To obtain the streaming-stage cells, cells were synchronously differentiated by 6-h cAMP pulsing. To obtain the slug-stage cells, cells incubated for 17–21 h on agar were collected, suspended in PB for dissociation by passing them through a syringe needle. Polydimethylsiloxane (PDMS) chambers were fabricated and used as described previously (61, 62). All fluorescence images were obtained by confocal microscopy. For details, see *SI Appendix*.

Plasmids, Protein Purification, and Microsphere Coating. His-tagged TgrB1^{ext} and TgrC1^{ext} expression vectors were constructed by inserting genomic DNA fragments of extracellular domain of *tgrB1* or *tgrC1* into the vector harboring *act15* promoter and His-tag sequence. Cells harboring pA15-tgrB1^{ext}-His$_6$-2H3term or pA15-tgrC1^{ext}-His$_6$-2H3term were designed to secrete extracellular domain of TgrB1 and TgrC1, respectively (*SI Appendix*, Fig. S1*C*). TgrB1^{ext} and TgrC1^{ext} were purified from the respective cultured medium by affinity chromatography using a Ni^{2+}-NTA column. Elution buffer was exchanged with PB by ultrafiltration. Purified TgrC1^{ext} was immobilized to functionalized silica beads (5 μm diameter, Sumitomo Bakelite BS-X9905) by covalent bond according to the manufacturer's protocol. For details, see *SI Appendix*.

ACKNOWLEDGMENTS. We thank S. Hirose, A. Kuspa, and G. Shaulsky for providing *tgrB1*$^-$, *tgrC1*$^-$, GFP/*tgrB1*$^-$, and tdTomato/*tgrC1*$^-$ strains and tgrB1/tgrC1 replacement vectors; M. Fukuzawa for pHygTm(+); R. H. Insall for PakBCRIB-RFP and HSPC300-GFP vectors; D. Knecht for the GFP-Lifeact vector; V. O. Nikolaev and M. J. Lohse for Epac1-camps; Yukako Asano, Taro Uyeda, Tom Egelhoff, and the Dicty Stock Center for pBig-GFP-Arp2 and pBig-GFP-Myo; Y. Shirokawa, M. Fujishiro, T. Adachi, and T. Sugita for technical assistance; and Joe Brzostowski for critical reading of an earlier draft. This work was supported by Ministry of Education, Culture, Sports, Science and Technology (MEXT) KAKENHI Grants JP18H04759 and JP16H01442; Japan Society for the Promotion of Science (JSPS) KAKENHI Grants JP17H01812 and JP15KT0076; and in part by MEXT KAKENHI Grant JP17H05992, JSPS KAKENHI Grant 25710022 25103008, Platform for Dynamic Approaches to Living System from MEXT and Japan Agency for Medical Research and Development (AMED), research grant from the Mitsubishi Foundation, Joint Research by Exploratory Research Center on Life and Living Systems (ExCELLS) Grant 18-204 (to S.S.), and JSPS Grant JP16K18537 (to A.N.). T.F. was supported by JSPS Fellowship Grant JP17J08690.

1. Cerchiari AE, et al. (2015) A strategy for tissue self-organization that is robust to cellular heterogeneity and plasticity. *Proc Natl Acad Sci USA* 112:2287–2292.
2. Xiong F, et al. (2013) Specified neural progenitors sort to form sharp domains after noisy Shh signaling. *Cell* 153:550–561.
3. Kay RR, Thompson CRL (2009) Forming patterns in development without morphogen gradients: Scattered differentiation and sorting out. *Cold Spring Harb Perspect Biol* 1: a001503.
4. Townes PL, Holtfreter J (1955) Directed movements and selective adhesion of embryonic amphibian cells. *J Exp Zool* 128:53–120.
5. Krens SFG, Heisenberg C-P (2011) Cell sorting in development. *Curr Top Dev Biol* 95: 189–213.
6. Foty RA, Pfleger CM, Forgacs G, Steinberg MS (1996) Surface tensions of embryonic tissues predict their mutual envelopment behavior. *Development* 122:1611–1620.
7. Graner F, Glazier JA (1992) Simulation of biological cell sorting using a two-dimensional extended Potts model. *Phys Rev Lett* 69:2013–2016.
8. Krieg M, et al. (2008) Tensile forces govern germ-layer organization in zebrafish. *Nat Cell Biol* 10:429–436.
9. Krens SFG, et al. (2017) Interstitial fluid osmolarity modulates the action of differential tissue surface tension in progenitor cell segregation during gastrulation. *Development* 144:1798–1806.
10. Méhes E, Vicsek T (2013) Segregation mechanisms of tissue cells: From experimental data to models. *Complex Adapt Syst Model* 1:4.
11. Yang X, Dormann D, Münsterberg AE, Weijer CJ (2002) Cell movement patterns during gastrulation in the chick are controlled by positive and negative chemotaxis mediated by FGF4 and FGF8. *Dev Cell* 3:425–437.
12. Wyngaarden LA, et al. (2010) Oriented cell motility and division underlie early limb bud morphogenesis. *Development* 137:2551–2558.
13. Tomchik KJ, Devreotes PN (1981) Adenosine 3′,5′-monophosphate waves in Dictyostelium discoideum: A demonstration by isotope dilution–fluorography. *Science* 212: 443–446.
14. Siegert F, Weijer CJ (1989) Analysis of optical density wave propagation and cell movement in the cellular slime mould Dictyostelium discoideum. *J Cell Sci* 93:325–335.
15. Sawai S, Thomason PA, Cox EC (2005) An autoregulatory circuit for long-range self-organization in Dictyostelium cell populations. *Nature* 433:323–326.
16. Gregor T, Fujimoto K, Masaki N, Sawai S (2010) The onset of collective behavior in social amoebae. *Science* 328:1021–1025.
17. Nakajima A, Ishihara S, Imoto D, Sawai S (2014) Rectified directional sensing in long-range cell migration. *Nat Commun* 5:5367.
18. Nicol A, Rappel W, Levine H, Loomis WF (1999) Cell-sorting in aggregates of Dictyostelium discoideum. *J Cell Sci* 112:3923–3929.
19. Clow PA, Chen T, Chisholm RL, McNally JG (2000) Three-dimensional in vivo analysis of Dictyostelium mounds reveals directional sorting of prestalk cells and defines a role for the myosin II regulatory light chain in prestalk cell sorting and tip protrusion. *Development* 127:2715–2728.
20. McQuade KJ, Nakajima A, Ilacqua AN, Shimada N, Sawai S (2013) The green tea catechin epigallocatechin gallate (EGCG) blocks cell motility, chemotaxis and development in Dictyostelium discoideum. *PLoS One* 8:e59275.
21. Traynor D, Kessin RH, Williams JG (1992) Chemotactic sorting to cAMP in the multicellular stages of Dictyostelium development. *Proc Natl Acad Sci USA* 89:8303–8307.
22. Vasiev B, Weijer CJ (1999) Modeling chemotactic cell sorting during Dictyostelium discoideum mound formation. *Biophys J* 76:595–605.
23. Matsukuma S, Durston AJ (1979) Chemotactic cell sorting in Dictyostelium discoideum. *J Embryol Exp Morphol* 50:243–251.
24. Chen G, et al. (2013) TgrC1 mediates cell-cell adhesion by interacting with TgrB1 via mutual IPT/TIG domains during development of Dictyostelium discoideum. *Biochem J* 452:259–269.
25. Hirose S, Santhanam B, Katoh-Kurosawa M, Shaulsky G, Kuspa A (2015) Allorecognition, via TgrB1 and TgrC1, mediates the transition from unicellularity to multicellularity in the social amoeba Dictyostelium discoideum. *Development* 142:3561–3570.
26. Dynes JL, et al. (1994) LagC is required for cell-cell interactions that are essential for cell-type differentiation in Dictyostelium. *Genes Dev* 8:948–958.
27. Sukumaran S, Brown JM, Firtel RA, McNally JG (1998) lagC-null and gbf-null cells define key steps in the morphogenesis of Dictyostelium mounds. *Dev Biol* 200:16–26.
28. Iranfar N, Fuller D, Loomis WF (2006) Transcriptional regulation of post-aggregation genes in Dictyostelium by a feed-forward loop involving GBF and LagC. *Dev Biol* 290: 460–469.
29. Siu CH, Des Roches B, Lam TY (1983) Involvement of a cell-surface glycoprotein in the cell-sorting process of Dictyostelium discoideum. *Proc Natl Acad Sci USA* 80: 6596–6600.
30. Hirose S, Benabentos R, Ho H-I, Kuspa A, Shaulsky G (2011) Self-recognition in social amoebae is mediated by allelic pairs of tiger genes. *Science* 333:467–470.
31. Hirose S, Chen G, Kuspa A, Shaulsky G (2017) The polymorphic proteins TgrB1 and TgrC1 function as a ligand-receptor pair in *Dictyostelium* allorecognition. *J Cell Sci* 130:4002–4012.
32. Jiang Y, Levine H, Glazier J (1998) Possible cooperation of differential adhesion and chemotaxis in mound formation of Dictyostelium. *Biophys J* 75:2615–2625.
33. Garrod DR (1974) The cellular basis of movement of the migrating grex of the slime mould Dictyostelium discoideum: Chemotactic and reaggregation behaviour of grex cells. *J Embryol Exp Morphol* 32:57–68.
34. Alvarez-Curto E, Weening KE, Schaap P (2007) Pharmacological profiling of the Dictyostelium adenylate cyclases ACA, ACB and ACG. *Biochem J* 401:309–316.
35. Kriebel PW, Barr VA, Parent CA (2003) Adenylyl cyclase localization regulates streaming during chemotaxis. *Cell* 112:549–560.
36. Huang C-H, Tang M, Shi C, Iglesias PA, Devreotes PN (2013) An excitable signal integrator couples to an idling cytoskeletal oscillator to drive cell migration. *Nat Cell Biol* 15:1307–1316.
37. Pollard TD, Borisy GG (2003) Cellular motility driven by assembly and disassembly of actin filaments. *Cell* 112:453–465.
38. Fukui Y, Kitanishi-Yumura T, Yumura S (1999) Myosin II-independent F-actin flow contributes to cell locomotion in dictyostelium. *J Cell Sci* 112:877–886.
39. Yoshida M, Stadler J, Bertholdt G, Gerisch G (1984) Wheat germ agglutinin binds to the contact site A glycoprotein of Dictyostelium discoideum and inhibits EDTA-stable cell adhesion. *EMBO J* 3:2663–2670.
40. Shaffer BM (1964) Intracellular movement and locomotion of cellular slime-mold amoebae. *Primitive Motile Systems in Cell Biology*, eds Allen RD, Kamiya N (Springer Netherlands, Dordrecht, The Netherlands), pp 387–405.
41. Dormann D, Weijer G, Parent CA, Devreotes PN, Weijer CJ (2002) Visualizing PI3 kinase-mediated cell-cell signaling during Dictyostelium development. *Curr Biol* 12: 1178–1188.
42. Umeda T, Inouye K (2002) Possible role of contact following in the generation of coherent motion of Dictyostelium cells. *J Theor Biol* 219:301–308.
43. Gerisch G, et al. (2009) Self-organizing actin waves as planar phagocytic cup structures. *Cell Adhes Migr* 3:373–382.
44. Maiuri P, et al. (2015) Actin flows mediate a universal coupling between cell speed and cell persistence. *Cell* 161:374–386.
45. Liu Y-J, et al. (2015) Confinement and low adhesion induce fast amoeboid migration of slow mesenchymal cells. *Cell* 160:659–672.
46. Benabentos R, et al. (2009) Polymorphic members of the lag gene family mediate kin discrimination in Dictyostelium. *Curr Biol* 19:567–572.
47. Lomakin AJ, et al. (2015) Competition for actin between two distinct F-actin networks defines a bistable switch for cell polarization. *Nat Cell Biol* 17:1435–1445.
48. Traynor D, Tasaka M, Takeuchi T, Williams J (1994) Aberrant pattern formation in myosin heavy chain mutants of Dictyostelium. *Development* 120:591–601.
49. Lam TY, Pickering G, Geltosky J, Siu CH (1981) Differential cell cohesiveness expressed by prespore and prestalk cells of Dictyostelium discoideum. *Differentiation* 20:22–28.
50. Andrew N, Insall RH (2007) Chemotaxis in shallow gradients is mediated independently of PtdIns 3-kinase by biased choices between random protrusions. *Nat Cell Biol* 9:193–200.
51. Chisholm RL, Firtel RA (2004) Insights into morphogenesis from a simple developmental system. *Nat Rev Mol Cell Biol* 5:531–541.
52. Saxe CL, 3rd, et al. (1993) CAR2, a prestalk cAMP receptor required for normal tip formation and late development of Dictyostelium discoideum. *Genes Dev* 7:262–272.
53. Glöckner G, et al. (2016) The multicellularity genes of dictyostelid social amoebas. *Nat Commun* 7:12085.
54. Carmona-Fontaine C, et al. (2008) Contact inhibition of locomotion in vivo controls neural crest directional migration. *Nature* 456:957–961.
55. Carmona-Fontaine C, et al. (2011) Complement fragment C3a controls mutual cell attraction during collective cell migration. *Dev Cell* 21:1026–1037.
56. Mayor R, Etienne-Manneville S (2016) The front and rear of collective cell migration. *Nat Rev Mol Cell Biol* 17:97–109.
57. Nakao S, Platek A, Hirano S, Takeichi M (2008) Contact-dependent promotion of cell migration by the OL-protocadherin-Nap1 interaction. *J Cell Biol* 182:395–410.
58. Cetera M, et al. (2014) Epithelial rotation promotes the global alignment of contractile actin bundles during Drosophila egg chamber elongation. *Nat Commun* 5: 5511.
59. Patsialou A, et al. (2013) Intravital multiphoton imaging reveals multicellular streaming as a crucial component of in vivo cell migration in human breast tumors. *Intravital* 2:e25294.
60. Li D, Wang Y-L (2018) Coordination of cell migration mediated by site-dependent cell-cell contact. *Proc Natl Acad Sci USA* 115:10678–10683.
61. Nakajima A, Ishida M, Fujimori T, Wakamoto Y, Sawai S (2016) The microfluidic lighthouse: An omnidirectional gradient generator. *Lab Chip* 16:4382–4394.
62. Nakajima A, Sawai S (2016) Dissecting spatial and temporal sensing in Dictyostelium chemotaxis using a wave gradient generator. *Methods Mol Biol* 1407:107–122.